23

Quality Assessments of Seafloor Mapping with Multibeam Echo Sounders

Jan Terje Bjørke[1,2] and Stein Nilsen[1]
[1]*Norwegian Defence Research Establishment,PO Box 115, N-3191 Horten,*
[2]*Norwegian University of Life Sciences, N-1432 Ås*
Norway

1. Introduction

Seafloor topography is often mapped by the use of multibeam echo sounders, see Figure 1 for illustration of the principle on measurement with multibeam echo sounders. These systems evolved from single beam systems twenty five years ago (Glittum et al., 1986) and are still in development in the direction of increased measurement precision, higher density of the sample points and higher number of measured data points per second. To ensure high quality of the measurements, the survey system must be regularly verified and calibrated, statistics about measurement errors derived, measurement quality monitored, spot checks of the surveyed area performed and identification of spikes, suspicious or unexpected observations carried out. Measurement errors can be divided into three classes: Systematic errors, random errors and outliers. Methodologies to perform the quality assessments considered, will be described and illustrated in some case studies. The final product in seafloor mapping is often a digital elevation model (DEM). From a DEM different cartographic products as contour line maps, perspective views, shaded relief maps or maps with coloured depth intervals can be derived. Digital elevation models can also be used in navigation of vessels, ships and boats or for the construction of technical installations in oil and gas winning. The range of applications of DEMs is therefore large. Since the construction of DEMs can be based on different interpolation techniques, an assessment of common methods will be presented.
Quality issues of spatial data are discussed in Guptill and Morrison (1995): *Spatial data quality is a key issue in an era where current electronic technologies and communications networks such as Internet allow easy access to digital data in spatial form.* Elements of spatial data quality are: (1) lineage, (2) positional accuracy, (3) attribute accuracy, (4) completeness, (5) logical consistency and (6) semantic accuracy. In the present chapter we will not cover all these aspects of spatial data quality, but we will illustrate some quality parameters with examples from seafloor mapping. These quality aspects are: (1) systematic and random measurements errors, (2) identification of unexpected observations and (3) accuracy of digital elevation models. The topics we will cover, belong to the following quality elements of Guptill and Morrison (1995): Positional accuracy, attribute accuracy and semantic accuracy.

2. Systematic measurement errors

Systematic errors in the measurement system should be detected and corrected before the survey is carried out. For this purpose we have developed a patented program system, SeaCal,

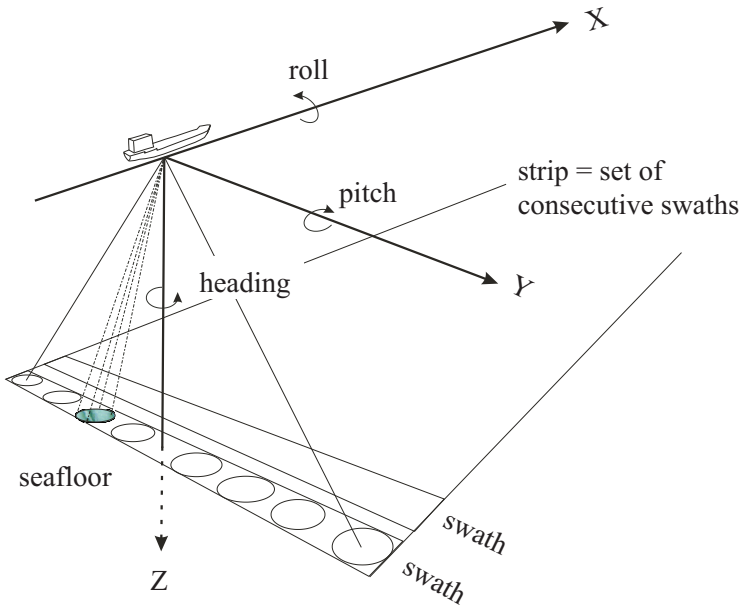

Fig. 1. Principle on measurement and coordinate axes of multibeam echo sounders. A fan of beams measures depth values on the seafloor. The coordinates of the measured points can for simplicity be explained as polar coordinates, i.e., they are computed from information about distance and direction from the centre of the measurement system to the seafloor.

that computes the calibration parameters from field measurements, see Bjørke (2004) and Bjørke (2005).

2.1 SeaCal

Systematic errors can be detected from field measurements by running several overlapping survey lines in different directions, see Figure 2. Static offsets in the three rotation angles—roll, pitch and heading—horizontal shift of the transducer relative to the reference point of the positioning system and systematic errors in the measured sound speed are derived simultaneously from the application of least-squares adjustment (Bjørke, 2005) as:

$$V = (A^T P_1 A)^{-1} A^T P_1 L_1, \tag{1}$$

where V is a vector of the unknown parameters, A a coefficient matrix, P_1 a weight matrix and L_1 a vector of observations. Since the stability of the system of equations depends on the relief of the seafloor and the configuration of the calibration lines, restrictions are put on the unknown parameters by

$$V = (A^T P_1 A + P_2)^{-1} (A^T P_1 L_1 + P_2 L_2), \tag{2}$$

where P_2 is a weight matrix of the unknown parameters and L_2 a vector of *a priori* parameter values; see for example Leick (1995). For example, in a flat area a small (differential) offset in the parameters often have no effect on the measured depth values and several parameters cannot med determined. Therefore, the stability conditions in Equation (2) are convenient to prevent numerical problems in the computations.

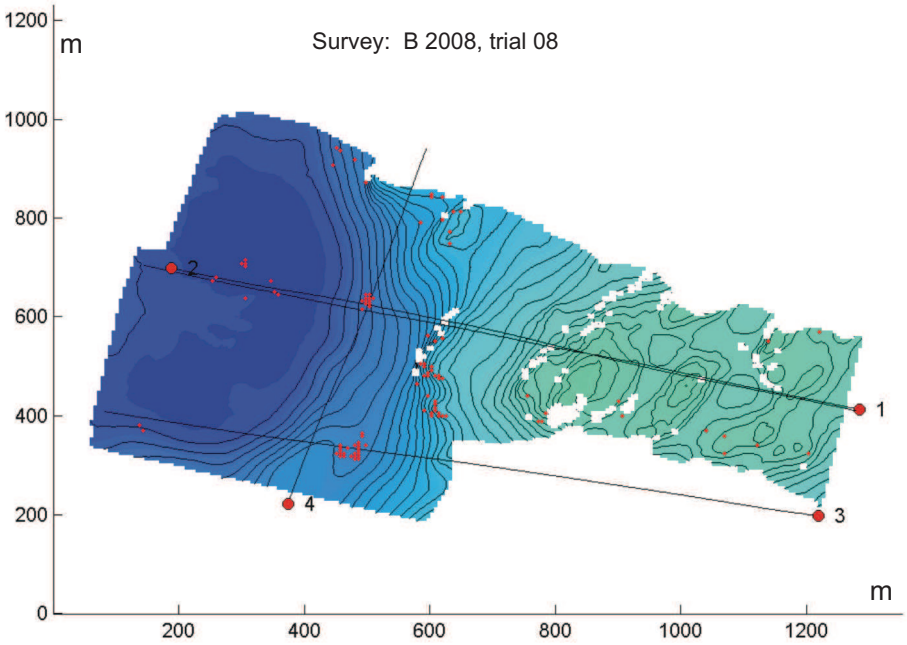

Fig. 2. Field calibration of multibeam echo sounder. The map shows the selected area, named B 2008, trial 08, with four calibration lines. There are three parallel lines and one crossing line. The sea depth varies from 85m to 244m.

The variance-covariance matrix of the unknowns can be computed from

$$Q_V = \sigma_0^2 (A^T P_1 A + P_2)^{-1}, \tag{3}$$

where σ_0^2 is the variance of the unit weight. Here, the diagonal elements define the variance of the parameters and the other elements their covariance. The variance $\sigma_{V_i}^2$ of parameter V_i is derived as

$$\sigma^2{}_{V_i} = Q_{V_{ii}},$$

and the covariance σ_{V_i,V_j} of the two parameters V_i and V_j is computed as

$$\sigma_{V_i,V_j} = Q_{V_{ij}}.$$

The correlation coefficient ρ_{V_i,V_j} measures how separable two parameters V_i and V_j are and is derived from Q_V as

$$\rho_{V_i,V_j} = \frac{\sigma_{V_i,V_j}}{\sigma_{V_i}\,\sigma_{V_j}}.$$

SeaCal utilizes the relation between horizontal movement and the corresponding change of the seafloor depth. This calibration methodology requires seafloor with some relief if all the static offset parameters of the transducer are to be computed.

The coefficient matrix A is defined in Table 1. Here, we suppose that the fan of beams is approximately in a vertical plane which are approximately perpendicular to the strip direction. The terrain slope is used to compute the change of the seafloor depth that corresponds to a certain horizontal movement. Rollscale is computed on the basis of Snell's law—-the law about refraction. Since ray tracing is not applied, it is assumed that a correction of the beam direction can be explained from changing the beam direction at the passage between the transducer and the water.
Snell's law can be written as

$$\phi_1 = \arcsin \frac{c_1}{c_0} \sin \phi_0 = \arcsin(k \ \sin \phi_0), \text{ where } k = \frac{c_1}{c_0};$$

c denotes the sound speed and ϕ the beam angle. We assume that $c_0 = 1500\text{m/sec}$ and get the relation between a small change dc_1 in sound speed and k as

$$dc_1 = 1500dk.$$

How a small change in k effects ϕ can be found from differentiation as

$$d\phi_1 = \frac{\sin \phi_0}{\sqrt{1 - k^2 \sin^2 \phi_0}} dk \approx \frac{\sin \phi_0}{\sqrt{1 - \sin^2 \phi_0}} dk \text{ when } k \approx 1. \tag{4}$$

We define

$$\Phi(\phi) = \frac{\sin \phi_0}{\sqrt{1 - \sin^2 \phi_0}} \tag{5}$$

and write Equation 4 as

$$d\phi_1 = \Phi(\phi) dk. \tag{6}$$

Factor dk will be termed rollscale factor.

name of parameter	small change of parameter	change in sea depth
roll	$\Delta\phi$	$[\partial H_y h - y]\Delta\phi$
pitch	$\Delta\omega$	$[-\partial H_x h]\Delta\omega$
heading	$\Delta\kappa$	$[\partial H_x y]\Delta\kappa$
translation in X	ΔX	$[\partial H_x]\Delta X$
translation in Y	ΔY	$[\partial H_y]\Delta Y$
relative tide correction	$\Delta h_i \ \forall$ strips	Δh_i
rollscale factor	Δk	$[\partial H_y h - y]\Phi(\phi)\Delta k$
horizontal scale factor	m_y	$[\partial H_y y]m_y$

Table 1. Definition of the calibration parameters in SeaCal. ∂H_x and ∂H_y are the terrain slope along the two horizontal axes, y the distance from the nadir point of the transducer to the measured point and h the vertical distance from the transducer to the measured point.

2.2 Field survey

The inspection of systematic errors of the multibeam echo sounder should be run on a regularly basis. For example, at the start and at the end of a survey, or as often as once a month. The length of the time period used to run the field measurements for the verification, is typically thirty minutes to one hour. Figure 2 shows measurements to control the calibration of a multibeam system. In this case four lines are measured in an area where the sea depth varies from 85m to 244m. The survey lines are each of length 1000m, approximately. The results of the calibration is shown in Figure 3. The table shows the corrections to be added to the different parameter settings. For example, roll should be corrected $+0.107^{\circ}$, the eccentricity of the transducer relative the GPS-antenna 1.84m in X-direction and -0.54m in Y-direction. The standard deviation of the depth measurements after the calibration is $\pm 0.11m$. The correlation between pitch and X is high, which says that in the present case the two parameters cannot be well separated. The reliability factor indicates how well the parameters can be computed. A red lamp signalises that the parameter considered should not be changed. In order to get a reliable value of this parameter, another calibration should be run—for example, find an area with a relieff that is more suited for field calibration of multibeam echo sounders.
Figure 4 illustrates the difference between a well calibrated multibeam echo sounder system and a system whithout a fine tuned calibration. The two graphs show the standard deviation of the depth measurements before and after the calibration is fine tuned. The calibration in Figure 2 is used for the construction of the two graphs. In the fine tuned case the standard deviation of the depth measurements is ± 0.11m against ± 0.49m in the case without fine tuning.

2.3 Error budget

From the contribution of the error sources defined in Table 1 an error budget can be set up. We assume the different error components are independent and compute their joint contribution σ by the law of variance propagation of random measurements. The error budget in Table 2 is computed for different beam angles and terrain slopes. The budget assumes sea depth 100m and certain values of the standard deviation of the different error sources. The important aspect of the computations is the exponential growth of σ as the beam angle increases. Therefore, for seafloor mapping with multibeam echo sounder the beam angle should be restricted to for example maximum 60°.

3. Computation of random measurement errors

Random measurement errors in multibeam echo sounder data are functions of the kind of measurement equipment used; the sea depth, the terrain slope and the weather conditions during the survey. Since the magnitude of the random measurement error may vary from one survey to another, efficient methods to derive this error component is attractive in quality control of the depth measurements. The method we have developed, makes it possible to derive the random measurement error from one single survey. This makes it possible to monitor the random measurement error during a survey, and random measurement errors can be derived without measuring the same area several times, which saves field work. Traditional methods, as for example proposed by Maas (2002), requires that the same area is measured twice. The method we launch, is based on the application of semivariogram modelling in geostatistical theory, see for example Cressie (1993); Olea (1999) or Wackernagel (1998) for an overview of geostatistical methods.

3.1 Application of theory from geostatistics

In geostatistics we consider terrain surfaces as realizations of random functions. The height Z in position u can then be defined as $Z = (u, \omega)$, where $u \in D \subset \mathbb{R}^2$. The letter ω denotes the

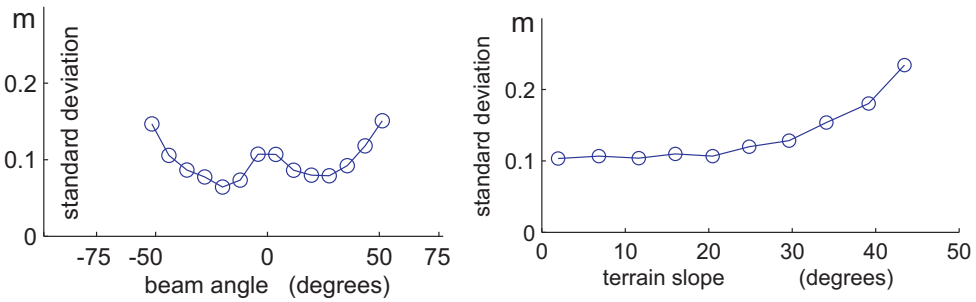

Calibration results

parameter	value	maximum correlation	reliability	fixed
roll	0.107	0.11	1.00	
pitch	0.033	0.94	0.94	
heading	0.003	-0.06	0.90	
x0	1.84	0.94	0.94	
y0	-0.54	-0.28	0.91	
h0	0.00	0.00	0.00	x
roll-scale	0.0007	0.11	0.84	
y-scale	0.0013	-0.28	0.95	

Standard deviation of the depth measurements after the calibration: 0.11

Legend

OK Evaluate Evaluation strongly recommended

Fig. 3. Field calibration of multibeam echo sounder from the survey shown in Figure 2. The graphs show how the precision of the measurements varies with beam angle and terrain slope. The table gives the results of the calibration computation, i.e, the parameter values, information about correlation and reliability. A red sign indicates that evaluation is recommended before the calibration values are entered into the system.

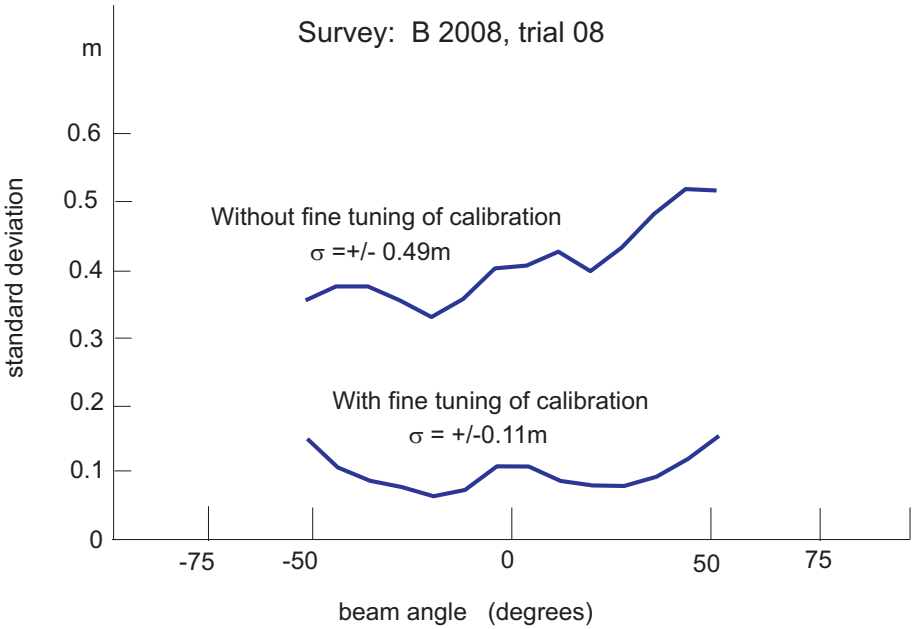

Fig. 4. Demonstration of the influence of not well calibrated multibeam echo sounder. Data used for the computation is the same as the data as used in Figure 3, i.e., survey B 2008, trial 08. The graphs show how the precision of the measurements varies with beam angle in the two cases: (1) the system is well calibrated and (2) the calibration is not fine tuned. The standard deviation of the residuals in the two cases is $\pm$0.11m and $\pm$0.49m, respectively.

particular realization, or outcome. For a fixed position u', $Z(u', \omega)$ is a random variable. For a fixed $\omega' \in \Omega$, $Z(u, \omega')$ is a deterministic function of u, called a realization of the random function.
Let $f(u) = Z(u, \omega')$ denote the exact terrain surface we are trying to model. We can write:

$$f(u) = m(u) + z(u),$$

where m is the *drift* and z a realization of a zero mean random function. The computation of the drift represents a challenge in geostatistics, see for example Olea (1999), page107, Cressie (1993), page 169 or Wackernagel (1998), page 213. Later on we will show how development of the mathematical theory of wavelets offers methods to compute approximations to the drift. The values we observe can be seen as samples of another surface

$$\tilde{f}(u) = m(u) + z(u) + w(u), \tag{7}$$

where w is assumed to be a zero mean white noise component due to measurement errors. In order to obtain an estimate of the random measurement errors of the multibeam echo sounder, $w(u)$ is the component we in this section want to compute; but first, we will deal with how to compute the drift.
The drift is defined as the expected value of a random function:

$$m(u) = E(Z) = \int_{\Omega} Z(u, \omega)\, dP(\omega), \tag{8}$$

	σ in meter					
Beam angle	Terrain slope					
	0°	10°	20°	30°	40°	50°
0°	± 0.10	± 0.11	± 0.13	± 0.17	± 0.23	± 0.30
5°	± 0.10	± 0.11	± 0.13	± 0.17	± 0.23	± 0.30
10°	± 0.10	± 0.11	± 0.13	± 0.17	± 0.23	± 0.31
15°	± 0.10	± 0.11	± 0.14	± 0.18	± 0.23	± 0.31
20°	± 0.11	± 0.11	± 0.14	± 0.18	± 0.24	± 0.32
25°	± 0.11	± 0.12	± 0.14	± 0.18	± 0.24	± 0.32
30°	± 0.11	± 0.12	± 0.15	± 0.19	± 0.25	± 0.33
35°	± 0.12	± 0.13	± 0.16	± 0.20	± 0.26	± 0.35
40°	± 0.13	± 0.14	± 0.17	± 0.21	± 0.28	± 0.37
45°	± 0.15	± 0.16	± 0.19	± 0.23	± 0.30	± 0.39
50°	± 0.17	± 0.18	± 0.21	± 0.26	± 0.32	± 0.43
55°	± 0.21	± 0.22	± 0.25	± 0.30	± 0.37	± 0.48
60°	± 0.27	± 0.28	± 0.31	± 0.36	± 0.43	± 0.55
65°	± 0.37	± 0.38	± 0.41	± 0.46	± 0.54	± 0.67
70°	± 0.57	± 0.58	± 0.60	± 0.65	± 0.74	± 0.88
75°	± 0.99	± 1.00	± 1.03	± 1.08	± 1.17	± 1.32
80°	± 2.20	± 2.21	± 2.24	± 2.29	± 2.39	± 2.56
85°	± 8.77	± 8.78	± 8.81	± 8.86	± 8.96	± 9.14

Table 2. Standard deviation of measured sea depth derived from the error budget. The sea depth is defined to 100m. The following error components are considered: Roll ($\sigma_\phi = \pm 0.05°$), pitch ($\sigma_\omega = \pm 0.1°$), heading ($\sigma_\kappa = \pm 0.1°$), error in measured sound speed at the transducer ($\sigma_v = \pm 1.0$m/sec) which corresponds to rollscale $\sigma_k = \pm 0.00067$, error in the measured position of the transducer in the three axis directions X ($\sigma_x = \pm 0.1$m), Y ($\sigma_y = \pm 0.1$m) and Z ($\sigma_z = \pm 0.1$m).

where $P(\omega)$ is the distribution function of ω. The procedure we will apply to approximate the drift, uses spatial averaging over subsets of D as proposed by Bjørke and Nilsen (2005) and Bjørke and Nilsen (2007).

We start the drift computation by dividing the geographical area into grid blocks, making sure a suitable number of measurements fall within each block; emphirical tests show that an average of approximately ten values per block gives good results. Based on these values, we estimate the average depth a_i inside each block and approximate the drift by generating the sum

$$m(u) = \sum_{j=1}^{n} a_j \, \phi_j(u), \tag{9}$$

where n is the number of blocks. Each function ϕ_j is continuous and has integral 1 over block j and integral zero over all other blocks. The method we use to construct these functions is based on average interpolating subdivision; for an introduction see Sweldens and Schröder (1996). Note that we are not interpolating the observations—the surface we construct has the same average values over the grid blocks as the original estimated values—and the surface does not in general pass through any of the measured data points. In the Appendix a C-implementation of the 2D-average interpolating algorithm is given.

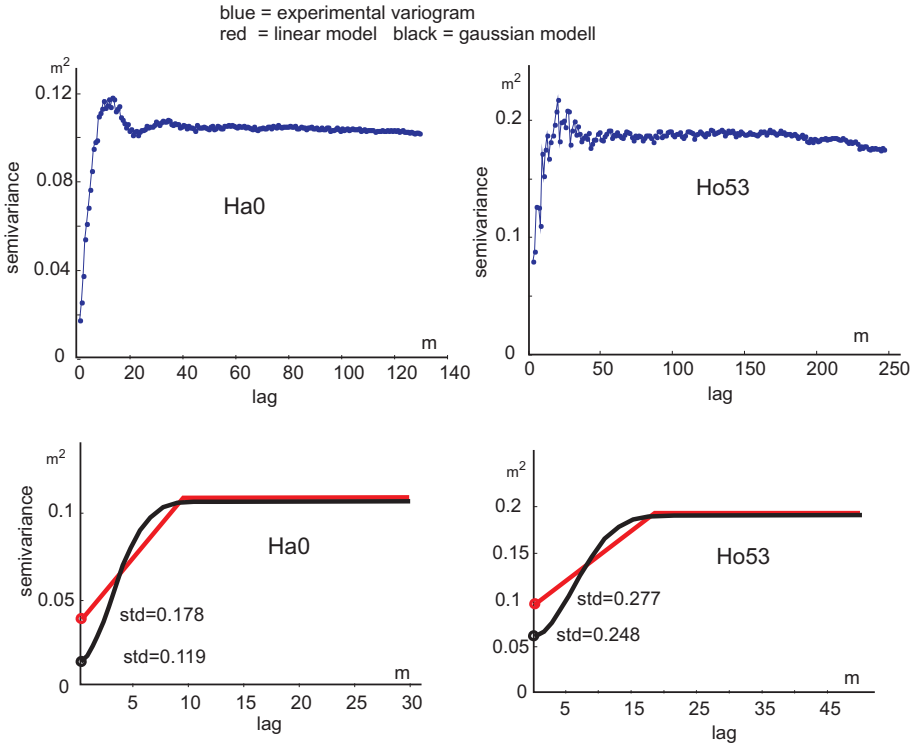

Fig. 5. Examples of experimental semivariogram and the fit of a linear and a Gaussian variogram model; note the parabolic form of the Gaussian variogram near the origin. Visually, one may expect the piecewise liner variogram to follow the linear part of the gaussian variogram more close. A reason for the discrepancy is that the curve fitting is computed from weighted least squares and that the number of observations in the lower part of the experimental variogram is small compared with the number of observations in the lag classes near the break point of the variogram.

When we have a model of the drift, we can compute the residuals between the drift and the observations as

$$r(u) = \tilde{f}(u) - m(u) = z(u) + w(u). \tag{10}$$

The two components $z(u)$ and $w(u)$ cannot be separated from these equations, but from the semivariogram we can derive $w(u)$. In the semivariogram $w(u)$ appears as the so-called nugget effect, see e.g. Olea (1999) or Cressie (1993).
The semivariogram is defined as

$$\gamma(h) = \frac{1}{2} E[\{r(u) - r(u+h)\}^2], \tag{11}$$

where u and $u+h$ are any two locations in the sample domain. The following expression is an unbiased estimator for the semivariogram

$$\tilde{\gamma}(h) = \frac{1}{2n(h)} \sum_{i=1}^{n(h)} \{r(u) - r(u+h)\}^2], \tag{12}$$

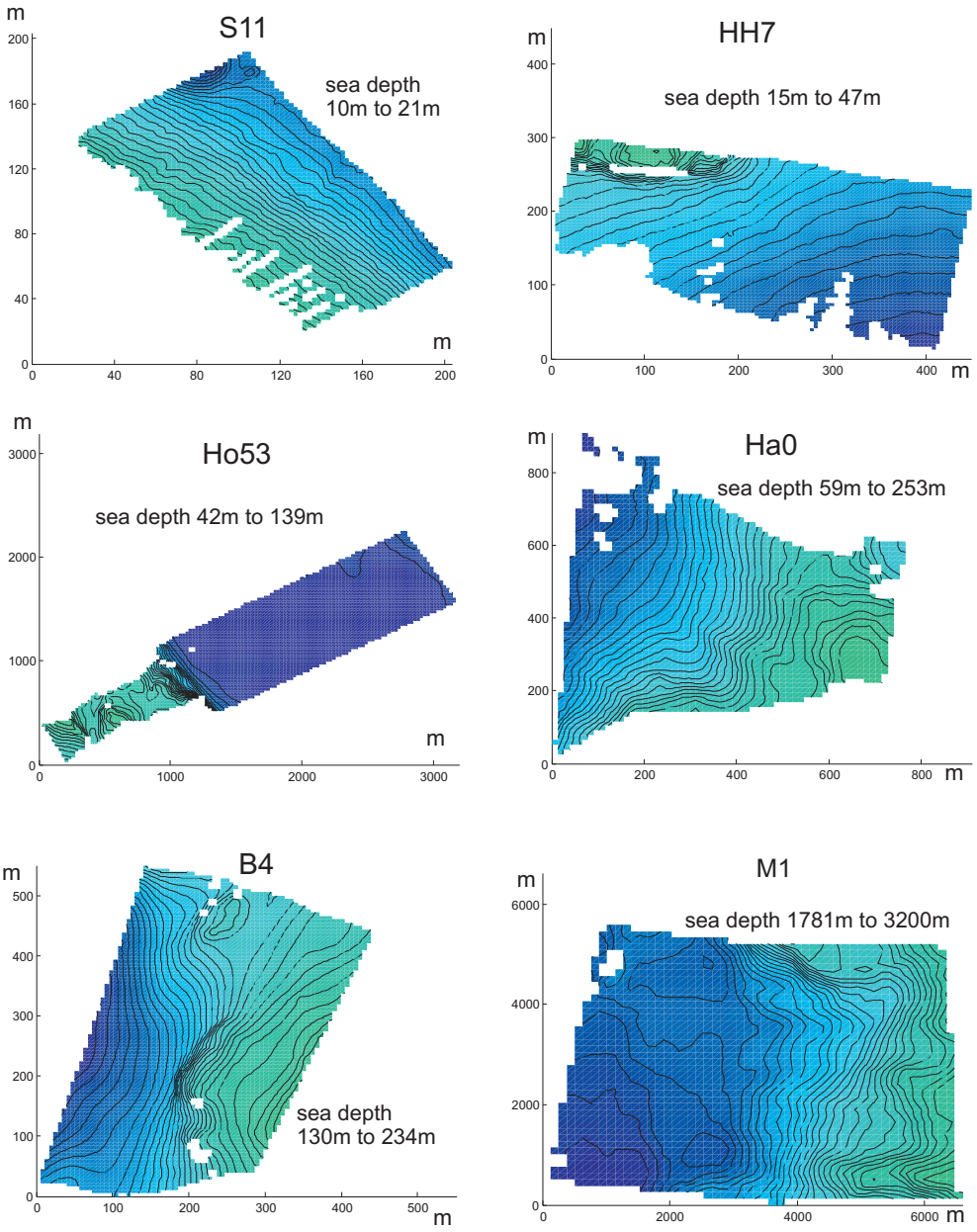

Fig. 6. Six maps of the twelve survey areas used for the study of random measurement errors of the multibeam echo sounder and for comparing different DEM-methods. Map S11 is also representative for survey S1, map HH7 representative for survey HH0 and so on.

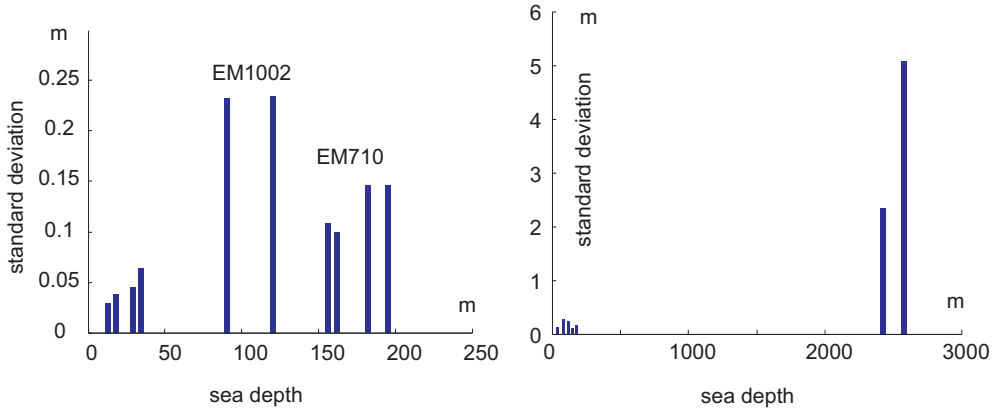

Fig. 7. Random errors of multibeam echo sounders used in the study areas. The values of σ_w are derived from the linear variogram as presented in Table 3. The kind of multibeam echo sounder used for the measurements is indicated, i.e., EM1002 and EM710; EM710 is a more modern system than EM1002.

where $n(h)$ is the number of pairs of variables at distance class h. Figure 5 shows two examples of experimental variograms. The number of permissible functions to be used for variogram fit is infinite, but in practice the options is reduced to a handful (Olea 1999, page 76). Some popular models are spherical, exponential, Gaussian, power and linear semivariogram models.
In the forthcoming experiments a linear and a Gaussian model will be used. The linear model is composed of two pieces. The first fits the part of the experimental variogram with small lags, and the next the rest of the variogram. Let h be the lag. Then the piecewise linear semivariogram is the model

$$\gamma(h) = \begin{cases} w + Ch \ , \ 0 < h \leq a \\ w + Ca \ , \ h > a, \end{cases} \tag{13}$$

where w is the noise and a the range, i.e., the lag at which the semivariogram reaches a constant value.

Let h be the lag. Then the Gaussian semivariogram is the model

$$\gamma(h) = w + C\left(1 - e^{-3(\frac{h}{a})^2}\right), \tag{14}$$

where w is the noise and a the range. The Gaussian semivariogram has a parabolic form near the origin. This property is useful when the noise of the measurements is to be computed. In many applications the noise is set to zero, but in our use of the variogram, the noise is a component we want to derive. Therefore, in the case of quality assessment of multibeam measurements, the ability of the variogram model to detect the noise, is important.
The standard deviation of the measurement errors can be derived from the variogram as

$$\sigma_w = \sqrt{\gamma(0)}, \tag{15}$$

see for example the explanation in Bjørke and Nilsen (2007) and the noise component as indicated in Figure 5. The variogram models are fitted by the use of least squares method

Survey	Sea depth	$\gamma(0)$	$\sigma_w = \sqrt{\gamma(0)}$		a	$\gamma(a)$	$\sigma_z = \sqrt{\gamma(a)}$
		linear	linear	Gaussian	linear	linear	linear
	m	m^2	m		m	m^2	m
S1	12-21	0.00181	±0.043	±0.038	1.8	0.00252	±0.050
S11	10-21	0.00121	±0.035	±0.029	1.6	0.00162	±0.040
HH0	18-43	0.00584	±0.076	±0.064	1.8	0.00717	±0.085
HH7	15-47	0.00398	±0.063	±0.045	1.7	0.00507	±0.071
Ho53	43-197	0.08879	±0.298	±0.235	17.4	0.19108	±0.437
Ho83	42-139	0.07188	±0.268	±0.233	12.0	0.09913	±0.315
Ha0	59-253	0.03719	±0.193	±0.108	9.3	0.10530	±0.325
Ha5	62-261	0.04562	±0.214	±0.100	11.8	0.16232	±0.403
B4	130-234	0.02791	±0.167	±0.146	3.6	0.03214	±0.179
B6	145-244	0.02938	±0.171	±0.146	4.7	0.04102	±0.203
M1	1781-3200	24.72150	±4.972	±4.964	84.8	32.76960	±5.725
M10	1780-3092	7.74608	±2.783	±2.473	85.8	17.94542	±4.236

Table 3. Computation of random measurement errors derived from the linear and the Gaussian semivariogram. In the table $\gamma(0)$ represents the variance of the random measurement errors and σ_w its standard deviation, i.e., $\sqrt{\gamma(0)}$. The value of the lag when the variogram reaches a constant value, is termed the range and denoted a. The corresponding value $\gamma(a)$ of the semivariogram is termed the sill. The square root of the sill approximates the standard deviation σ_z of the residuals.

where the number of observations in each lag class is used as weights such that more observations gives higher weight. When the Gaussian model is computed, one should watch for invalid solutions; visual presentation of the variogram model is recommended. One should also test for invalid semivariograms, for example, if the least squares curve fitting gives negative semivariance at the origin.

3.2 Demonstration of the computation of random measurement errors

Computation of random measurement errors from the experimental semivariogram will be derived from the twelve surveys illustrated in Figure 6. By applying Equation 15 to the two variogram models in Figure 5, we find that in area Ha0 σ_w is ±0.178 for the linear variogram and ±0.119 for the Gaussian variogram. In area Ho53 the linear and the Gaussian variogram give σ_w is ±0.277 and ±0.248, respectively. This indicates that the Gaussian variogram may give lower values for σ_w than the linear variogram. Note the parabolic form of the Gaussian model near the origin.

Table 3 shows the results from applying the linear and the Gaussian variogram models to the data in the twelve test areas. The standard deviation of the random measurement errors increases with increasing sea depth. In the shallow water areas σ_w is some centimeters and is of the magnitude several meters in the deep water areas. The range a represents the correlation distance. For lags less than a, the residuals are correlated. The value of a varies

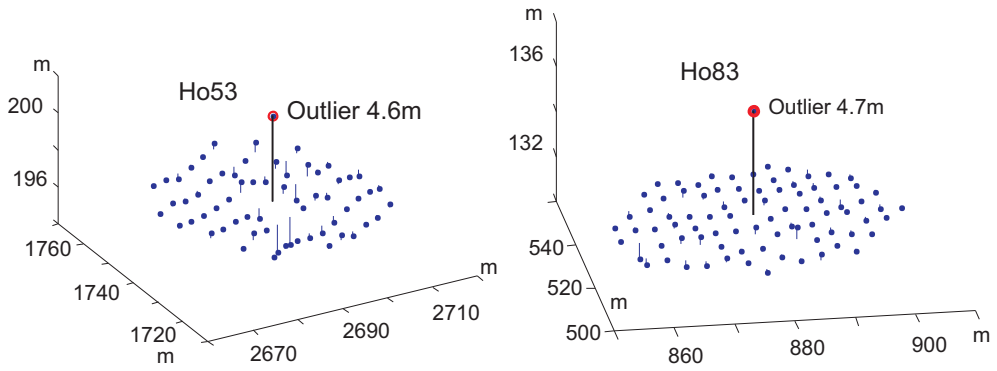

Fig. 8. Identification of isolated outliers

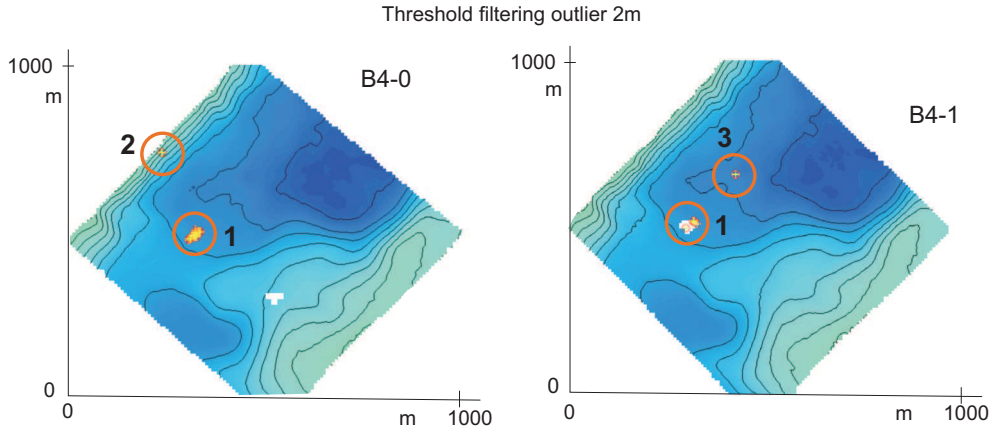

Fig. 9. Outliers identified in two surveys of the same area. In the red circle numbered 1 there are unexpected observations in both the surveys. The vertical distance between the contour lines is 5m

from approximately two meter in the shallow water area and up to almost one hundred meter in the deep water area. We notice that σ_w systematically is lower for the Gaussian model than the linear model. In a coming section on quality of digital elevation models the discrepancies between the two models will be discussed. The conclusion from this evaluation is that the Gaussian model seems to give more reliable semivariograms than the linear model.

Figure 7 shows how the random measurement error varies with the sea depth. The main impression is that σ_w increases with increasing sea depth, but at depth 100m there are two surveys—Ho53 and Ho83—that show higher value of σ_w than surveys at depth 150m to 200m. This can be explained from the survey equipment used. For Ho53 and Ho83 multibeam echo sounder EM1002 is used, and in the other case EM710 is applied. Since EM710 belongs to a newer generation multibeam echo sounders than EM1002, the measurement precision of EM710 is improved compared with the precision of EM1002. This explains why Figure 7 does not show a monotonic increasing relation between σ_w and increasing sea depth.

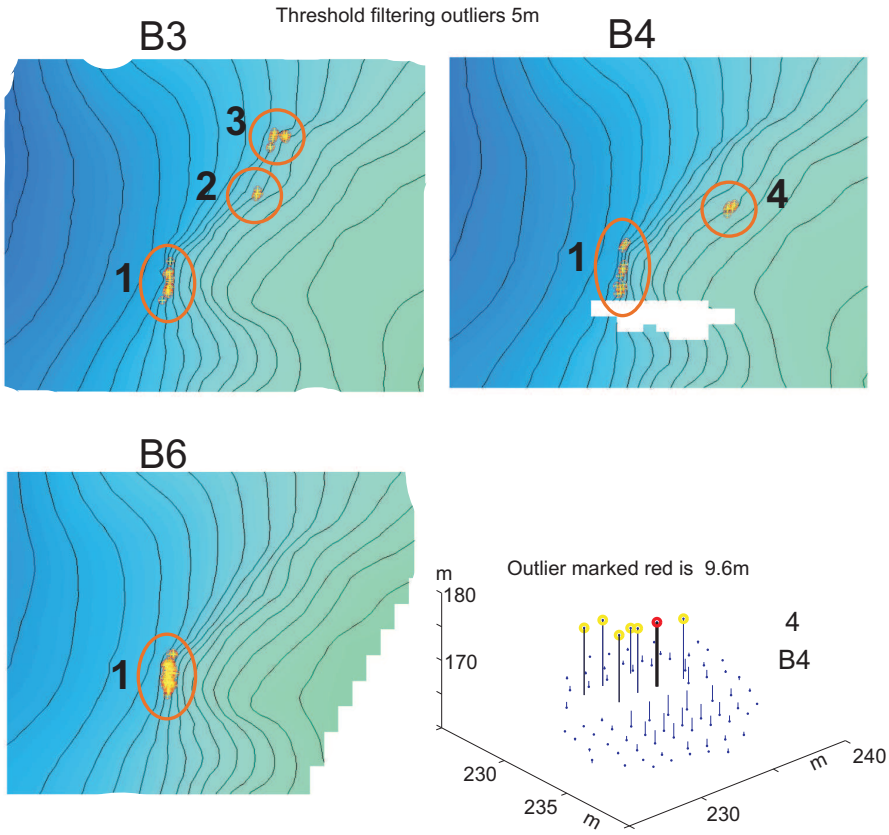

Fig. 10. Outliers identified in three surveys of the same area. In the red circle numbered 1 there are unexpected observations in all the surveys. The vertical distance between the contour lines is 5m. A perspective view of outliers in circle 4 in survey B4 is shown.

4. Detection of outliers in the measurements

Some case studies will illustrate the detection and the interpretation of outliers in depth measurements with multibeam echo sounder. We define an outlier as an unexpected large residual between the drift surface and the measured depth values. Unexpected large may be set to a threshold derived from the standard deviation σ of the residuals, for example 6σ. In the selected test areas the portion of the residuals greater than 6σ is less than 0.1% of the number of measured depth points. Average interpolation wavelets algorithm will be used for the drift computation, see the Appendix for description of this method. The average interpolation wavelets algorithm is well suited for detection of outliers, because average values are resistant against large measurement errors.

Figure 8 illustrates the detection of isolated outliers in the two surveys Ho53 and Ho83. In both cases the outlier is of magnitude 4m-5m. A question is: Can these unexpected observations be regarded as measurement errors?. For example, is there a human construction on the seafloor that have caused the spike or have we detected a ship wreck? In principle, we need more information to classify an outlier as a huge measurement error. Knowledge of properties of the

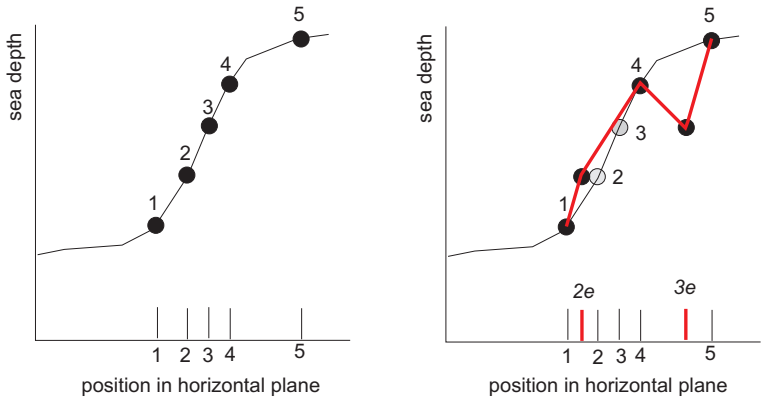

Fig. 11. Demonstration on how a horizontal position error may effect a measured terrain profile. In the first case we assume no position error. In the second case point 2 is associated to position 2e and point 3 to position 3e. The other terrain points in the second case are associated to their correct positions. The red profile line shows how the position errors have changed the profile from a monotonic increasing profile to a profile with a sharp local minima.

measurement system, weather conditions during the survey and other additional information will be of value when outliers are to be evaluated.
In Figure 9 the same area is measured twice. This gives us more information about the outliers compared with information from one single measurement of the seafloor. The red circles in Figure 9 mark areas with outliers. As we can see, the area numbered 1 occur in both surveys. Therefore, this indicates that there may be some terrain features in this area that cause the unexpected observations.
Figure 10 shows three surveys of the same area. Also in this case there are areas with outliers that are marked in all the tree surveys, see the circle numbered 1. The outliers in circle 4 in survey B4 are illustrated in the perspective view. A group of outliers of size 10m, approximately, occurs in an area of size 8m$\times$8m.
Figure 11 demonstrates how a horizontal position error may effect a measured terrain profile. In the first case we assume no position error. In the second case point 2 is associated to position 2e and point 3 to position 3e. The other terrain points in the second case are associated to their correct positions. The red profile line shows how the position errors have changed the profile from a monotonic increasing profile to a profile with a sharp local minima.
The identification of outliers in the depth measurements raises several questions of how these measurements should be treated:

1. Should the measurments classified as outliers be removed from the data set?;
2. should the area with the outliers be inspected by new measurements?;
3. should the trend surface be used as a substitute for the measured data points?;
4. how to implement a system for automated detection and elimination of outliers?;
5. and how to design the user interaction in an automated system for handling of outliers.

Therefore, there are research question to be answered when an automated system for elimination of outliers are to be realized.

5. Quality of interpolation methods in digital elevation models

A product from seafloor mapping is often digital elevation models (DEMs). From a DEM different cartographic products as contour line maps, perspective views, shaded relief maps or maps with coloured depth intervals can be derived. Digital elevation models can also be used in navigation of vessels, ships and boats or for the construction of technical installations in oil and gas winning. The range of applications of DEMs is therefore large. Since the construction of a DEM can be based on different interpolation methods, an assessment of common interpolation methods will be presented. The methods we will investigate is average interpolation wavelets, triangle methods (TIN), moving surface and kriging. A brief description of these methods will be presented before we run the experiment.

5.1 Average interpolating wavelets

Average interpolating wavelets was presented in Section 3; see this section and the Appendix where a C implementation of the 2D-average interpolating wavelets algorithm is given..

5.2 TIN

Triangle models are often used in digital terrain models. The method is frequently referenced as triangulation irregular network (TIN). The construction principle of the network follows the so-called Delaunay principle. There exist several methods for the computation of a Delaunay triangulation of a set of points, see for example Kreveld (1997). When the triangles are computed, interpolation of depth values in a point with coordinates (x, y) is carried out from the linear interpolation

$$z(x, y) = a_1 + a_2 x + a_3 y,$$

where the coefficients are computed on the basis of the depth value in the three corners of the circumscribing triangle of the point considered.

5.3 Moving surface

Moving surface interpolates the depth z in position (x, y) from a polynomial. In our application we select coefficients from the bi-cubic polynomial

$$\begin{aligned} z(x, y) = {} & a_1 + a_2 x + a_3 y + a_4 xy + \\ & a_5 x^2 + a_6 y^2 + a_7 x^2 y + a_8 x y^2 + a_9 x^2 y^2 + \\ & a_{10} x^3 + a_{11} y^3 + a_{12} x^3 y \\ & + a_{13} x y^3 + a_{14} x^3 y^2 + a_{15} x^2 y^3 + a_{16} x^3 y^3; \end{aligned} \tag{16}$$

which can be written as

$$z(u) = \sum_{j=1}^{k} a_j b_j(u) \tag{17}$$

where k is the number of coefficients of the polynomial and $b_j(u)$ a function of the (x, y) coordinates of point u.

The coefficients a_j of the polynomial is derived by applying least squares approximation to the data points in a neighbourhood of the point to be interpolated. This requires the following system of equations to be solved:

$$\mathbf{v} = \mathbf{f} - \mathbf{B}\boldsymbol{\Delta},$$

where

$$\mathbf{v} = \begin{bmatrix} v_1 \\ v_2 \\ \vdots \\ v_n \end{bmatrix}; \mathbf{f} = \begin{bmatrix} z_1 \\ z_2 \\ \vdots \\ z_n \end{bmatrix}; \mathbf{B} = \begin{bmatrix} b_1(u_1) & b_2(u_1) & \cdots & b_k(u_1) \\ b_1(u_2) & b_2(u_2) & \cdots & b_k(u_2) \\ \vdots & \vdots & \vdots & \vdots \\ b_1(u_n) & b_2(u_n) & \cdots & b_k(u_n) \end{bmatrix} \text{ and } \mathbf{\Delta} = \begin{bmatrix} a_1 \\ a_2 \\ \vdots \\ a_k \end{bmatrix};$$

$$\text{such that } \sum_{i=1}^{n} p_i v_i v_i = \min. \tag{18}$$

Here,

p_i is the weight of data point u_i;

n is the number of data points;

k is the number of coefficients to be computed;

$\mathbf{f}$ is a vector of observed depth values;

$\mathbf{\Delta}$ is a vector of the coefficients to be computed;

and $\mathbf{B}$ is a matrix of variables defined in Equations 16 to 17 such that $b_j(u_i)$ is variable j for data point i.

Weight p_i is computed from the euclidian distance $d(\cdot)$ between point q_0 to be interpolated and its neighbouring point q_i as

$$p_i = \frac{1}{\epsilon + (d(q_0, q_i))^2},$$

where ϵ is a small positive number to prevent division by zero. By defining P as a $n \times n$ weight matrix as

$$\mathbf{P} = \begin{bmatrix} p_1 & 0 & 0 & \cdots & 0 \\ 0 & p_2 & 0 & \cdots & 0 \\ 0 & 0 & p_3 & \cdots & 0 \\ \vdots & \vdots & \vdots & \vdots & \vdots \\ 0 & 0 & 0 & \cdots & p_n \end{bmatrix},$$

the solution for $\mathbf{\Delta}$ is

$$\mathbf{\Delta} = \mathbf{N}^{-1}\mathbf{t}, \text{ where } \mathbf{N} = \mathbf{B}^t\mathbf{P}\mathbf{B} \text{ and } \mathbf{t} = \mathbf{B}^t\mathbf{P}\mathbf{f}. \tag{19}$$

5.4 Kriging

The roots of kriging goes back to pioneering work seventy years ago. Kriging is a form of generalized regression for the formulation of a minimum square error sense. There are several forms of kriging: Simple kriging, ordinary kriging, universal kriging, block kriging and other forms. In our experiment we will apply simple kriging and universal kriging. Details of the kriging equations are well covered in geostatistical literature, for example, Olea (1999) gives a presentation well suited to be read by engineers. Therefore, only a summary of the kriging equations will be given in the present paper.

5.4.1 Simple kriging

Simple kriging requires knowledge of the drift $m(u)$ and the semivariogram $\gamma(h)$ of the residuals $r(u)$ between the drift and the observations $\tilde{f}(u)$, see Equationes 10 and 12. The simple kriging equations take the form

$$\mathbf{MA} = \mathbf{S}, \tag{20}$$

where

$$\mathbf{M} = \begin{pmatrix} \gamma(u_1,u_1) & \gamma(u_1,u_2) & \cdots & \gamma(u_1,u_k) \\ \gamma(u_2,u_1) & \gamma(u_2,u_2) & \cdots & \gamma(u_2,u_k)) \\ \vdots & \vdots & \vdots & \vdots \\ \gamma(u_k,u_1) & \gamma(u_k,u_2) & \cdots & \gamma(u_k,u_k) \end{pmatrix}$$

and

$$\mathbf{A} = (\lambda_1\ \lambda_2\ \cdots \lambda_k)^t \text{ and } \mathbf{S} = \gamma(u_1,u_0)\ \gamma(u_2,u_0)\ \cdots \gamma(u_k,u_0)^t.$$

The interpolated value in u_0 is derived from

$$\hat{f}(u_0) = \sum_{j=1}^{k} \lambda_j r(u_j) + m(u_0),$$

which expresses that that the interpolated value is computed from a linear kombination of the residuals in the neighbouring data points.

In simple kriging the variance in the interpolated point is computed as

$$\sigma^2 = \mathbf{A}^t\mathbf{S}. \tag{21}$$

5.4.2 Universal kriging

Universal kriging does not require knowledge of the drift, but the semivariogram of the residuals between the drift and the observations must be known. Therefore, determination of the semivariogram may in universal kriging also require knowledge of the drift. The equations in universal kriging represents a generalization of the equations of simple kriging and takes the form

$$\mathbf{CV} = \mathbf{F} \tag{22}$$

where

$$\mathbf{C} = \begin{pmatrix} \gamma(u_1,u_1) & \gamma(u_1,u_2) & \cdots & \gamma(u_1,u_k) & b_1(u_1) & b_2(u_1) & \cdots & b_n(u_1) \\ \gamma(u_2,u_1) & \gamma(u_2,u_2) & \cdots & \gamma(u_2,u_k) & b_1(u_2) & b_2(u_2) & \cdots & b_n(u_2) \\ \vdots & \vdots & \vdots & \vdots & \vdots & \vdots & \vdots & \vdots \\ \gamma(u_k,u_1) & \gamma(u_k,u_2) & \cdots & \gamma(u_k,u_k) & b_1(u_k) & b_2(u_k) & \cdots & b_n(u_k) \\ b_1(u_1) & b_1(u_2) & \cdots & b_1(u_k) & 0 & 0 & \cdots & 0 \\ b_2(u_1) & b_2(u_2) & \cdots & b_2(u_k) & 0 & 0 & \cdots & 0 \\ \vdots & \vdots & \vdots & \vdots & \vdots & \vdots & \vdots & \vdots \\ b_n(u_1) & b_n(u_2) & \cdots & b_n(u_k) & 0 & 0 & \cdots & 0 \end{pmatrix}$$

and

$$\mathbf{V} = [\lambda_1\ \lambda_2\ \cdots \lambda_k\ \mu_1\ \mu_2\ \cdots \mu_n] \text{ and } \mathbf{F} = [\gamma(u_1,u_0)\ \gamma(u_2,u_0)\ \cdots \gamma(u_k,u_0)\ b_1(u_0)\ b_2(u_0)\ \cdots b_n(u_0)].$$

The parameters λ_i are Lagrange multipliers to ensure that universal kriging becomes an unbiased estimator. The drift is represented by the coefficients $b(u)$. In our implementation we have taken them from the bi-cubical ploynomial in Equation 17. How many coefficients that are used, is decided from the number of data points in the neighbourhood of the point to be estimated.

The interpolated value in u_0 is derived from

$$\hat{f}(u_0) = \sum_{j=1}^{k} \lambda_j \tilde{f}(u_j).$$

In universal kriging the variance in the interpolated point is computed as

$$\sigma^2 = \mathbf{V}^t \mathbf{F}. \tag{23}$$

When solving kriging equations, one should be aware of possible *numerical problems*, see for example Davis and Morris (1997). For example, if two points have identical coordinates, they will produce equal kriging equations, and the system of equations will become singular.

5.5 Evaluation of the interpolation methods

Computation of interpolation errors of different interpolation methods will be derived from the twelve surveys as indicated in Figure 6. A portion of the sample points are selected as control points. This subset C is subtracted from the original data set A, and a new set B is derived as $B = A \setminus C$. Set B is used for the interpolation of depth values in the points of C. The residuals between the measured and the interpolated depth values of set C is computed. Interpolation methods to be investigated are simple and universal kriging, TIN, moving surface and wavelets. The results of the computations are shown in Table 4. In nine cases the variation of the standard deviation in the control points for the different interpolation methods is less than 10%. In one case the variation is of magnitude 30% and in two cases 100%. In seven cases universal kriging performs better than TIN and equal in five. Moving surface works better than TIN in six cases, equal in four and weaker two cases. Average interpolating wavelets performs better than TIN in two cases, equal in one and weaker in nine cases. Ranking the methods on basis of the standard deviation in the control points gives:

1. Universal kriging,
2. simple kriging,
3. moving average,
4. TIN,
5. and average interpolating wavelets.

An attractive property of kriging is its ability to estimate the variance of the interpolated depth values. From Equation 23 the average kriging variance σ_u^2 in the control points of the twelve survey areas can be derived. The results of these computations are presented in Table 5. The realism of σ_u^2 depends on how well the variogram is modelled. An evaluation of σ_u^2 will be carried in the following. The residual $r(u)$ between the measured value $\tilde{f}(u)$ and universal kriging value $g(u)$ in point u is

$$r(u) = \tilde{f}(u) - g(u).$$

From the law of variance propagation of independent measurements we can compute the variance $\hat{\sigma}_r^2$ of $r(u)$ as

$$\hat{\sigma}_r^2 = \sigma_w^2 + \sigma_u^2,$$

Survey	Sea depth m	Simp. kr. m	Univ. kr.. m	TIN m	Mov. surf. m	Wavelets m
S1	12-21	±0.045	±0.044	±0.045	±0.044	±0.051
S11	10-21	±0.041	±0.041	±0.041	±0.040	±0.044
HH0	18-43	±0.052	±0.053	±0.073	±0.067	±0.078
HH7	15-47	±0.057	±0.058	±0.060	±0.059	±0.074
Ho53	43-197	±0.316	±0.304	±0.317	±0.277	±0.381
Ho83	42-139	±0.275	±0.285	±0.301	±0.259	±0.304
Ha0	59-253	±0.152	±0.144	±0.146	±0.178	±0.324
Ha5	62-261	±0.155	±0.151	±0.148	±0.196	±0.388
B4	130-234	±0.175	±0.180	±0.204	±0.175	±0.183
B6	145-244	±0.168	±0.166	±0.175	±0.165	±0.191
M1	1781-3200	±6.259	±0.6.084	±6.201	±5.098	±5.494
M1	1780-3092	± 3.302	±3.245	±3.437	± 2.876	± 4.138

Table 4. Standard deviation for different interpolation methods. The standard deviation is computed from the residuals between measured depth value and interpolated value in the control points.

Survey	σ m	Survey	σ m
S1	±0.043	Ha0	±0.194
S11	±0.036	Ha5	±0.222
HH0	±0.078	B4	±0.169
HH7	±0.063	B6	±0.174
Ho53	±0.306	M1	±5.124
Ho83	±0.265	M10	±2.759

Table 5. Average standard deviation of depth values computed from universal kriging variance, see Equation 23

where the noise component σ_w^2 of the measurements can be derived from the semivariogram and the universal kriging variance σ_u^2 by the application of Equation 23. The variance of $r(u)$ can also be computed from the residuals in the control points as

$$\sigma_r^2 = \frac{1}{n}\sum_{i=1}^{n}(\tilde{f}(u) - g(u))^2,$$

where $\tilde{f}(u)$ is the measured depth value in u and the $g(u)$ the value computed from universal kriging and n the number of control points. From the standard deviation of the two variances the relation

$$q = \frac{\hat{\sigma}_r}{\sigma_r} \tag{24}$$

is computed and presented in Table 6.

Survey	Gaussian	linear	Survey	Gaussian	linear
S1	1.30	1.38	Ha0	1.54	1.90
S11	1.12	1.22	Ha5	1.61	2.04
HH0	1.90	2.05	B4	1.24	1.32
HH7	1.33	1.54	B6	1.37	1.47
Ho53	1.27	1.41	M1	1.17	1.17
Ho83	1.24	1.32	M10	1.14	1.21
mean value				1.35	1.50

Table 6. Factor computed to evaluate the realism of the kriging variance in the control points, see Equation 24. The factor is computed for both the Gaussian and linear semivariogram given in Table 3. The closer the factor is to 1, the more realistic the semivariogram is modelled.

From Table 6 we can see that the Gaussian and the linear semivariogram on average give q-factor 1.35 and 1.50, respectively. The closer the factor is to 1, the more realistic the kriging variance will be. Therefore, the Gaussian semivariogram gives slightly more realistic values of the kriging variance than the linear semivariogram. The Gaussian variogram seems therefore to be preferable when applied to seafloor mapping from multibeam echo sounder measurments.

6. Conclusions

Quality issues of spatial data are illustrated by examples from seafloor mapping with multibeam echo sounder. The methodologies to compute systematic errors and random errors of the multibeam echo sounders represent rather new approaches—although, well known techniques as least squares adjustment and geostatistical tools are applied. The average interpolating wavelets algorithm shows its strength in the computation of the drift of seafloor models, and we have demonstrated how the drift is used to derive residuals for the computation of random errors, outliers and the semivariogram used in kriging interpolation. We have shown how the three error components—random measurement errors, systematic errors and outliers—can be identified from depth measurements with multibeam echo sounders. Since these error sources are important to the quality of seafloor maps and digital elevation models, their parameters should be documented and follow the measurements as so-called *metadata*.
Different interpolation methods are compared. These methods can be used to compute digital terrain models with regular sampling patterns from scattered data. Grid models, for example, have regular sampling pattern and are very popular computer representations of digital elevations models. The interpolation methods investigated, are selected from the class of models often used in seafloor mapping. The general impression of the comparison is kriging interpolation shows slightly higher precision than the other methods. For practical purposes we recommend that factors as *speed of computation and numerical stability* should be considered when interpolation methods are to be implemented.

7. Acknowledgements

This research is supported by FFI-projects 113602 and 113002.

8. References

Bjørke, J. T.: 2004, En metode for feltkalibraring av systemparametere i et multistråleekkolodd-system (Eng. a method for field calibration of system parameters in a multibeam echo sounder system), Norwegian patent no. 315766, Norwegian Patent Office, PO Box 8160 Dep. 0033, Oslo, Norway.

Bjørke, J. T.: 2005, Computation of calibration paramters for multibeam echo sounders using least squares method, *IEEE Jornal of Oceanic Engineering* 30(4), 818–831.

Bjørke, J. T. and Nilsen, S.: 2002, Efficient representation of digital terrain models: compression and spatial decorrelation techniques, *Computers & Geosciences* 28, 433–445.

Bjørke, J. T. and Nilsen, S.: 2003, Wavelets applied to simplification of digital terrain models, *International Journal of Geographical Information Science* 17(7), 601–621.

Bjørke, J. T. and Nilsen, S.: 2005, Trend extraction using average interpolating subdivision, *Mathematical Geology* 37(6), 615–634.

Bjørke, J. T. and Nilsen, S.: 2007, Computation of random errors i digital terrain models, *Geoinformatica* 11, 359–382.

Bjørke, J. T. and Nilsen, S.: 2009, Fast trend extraction and identification of spikes in bathymetric data, *Computers & Geosciences* 35, 1061–1071.

Cressie, N. A. C.: 1993, *Statistics for Spatial Data, Revised Ed.*, Probability and Mathematical Statistics, John Wiley & Sons, Inc., New York. 900 pp.

Davis, G. J. and Morris, M. D.: 1997, Six factors which affect the condition number of matrices associated with kriging, *Mathematical Geology* 29(5), 669–683.

Glittum, M., Heier, O., Pohner, F. and Vestgard, K.: 1986, Multibeam echo-sounder system for sea bed mapping, *Oceanology: Proceedings of an international conference, March 4 - 7, 1986, Brighton, UK*, Advances in Underwater Technology and Offshore Engineering. Oceanology, Volume 6, The Society for Underwater Technology. ISBN 0-86010-772-8.

Guptill, S. C. and Morrison (editors), J. L.: 1995, *Elemenst of spatial data quality*, Elsevier Science Ltd., Oxford, U.K.

Kreveld, M. J. v.: 1997, Digital elevation models and TIN algorithms, *in* M. J. Kreveld, J. Nievergelt, T. Roos and P. Widmayer (eds), *Algorithmic foundations of geographical information systems*, Vol. 1340 of *Lecture Notes in Computer Science*, Springer-Verlag, London,UK, pp. 37–78. ISBN 3-540-63818-0.

Leick, A.: 1995, *GPS: Satellite surveying*, second edn, John Wiley & Sons. Inc., USA.

Maas, H.-G.: 2002, Methods for measuring height and planimetry discrepances in airborne laserscanner data, *Photogrammetric Engineering & Remote Sensing* 68(9), 933–940.

Olea, R. A.: 1999, *Geostatistics for Engineers and Earth Scientists*, Kluwer Academic Publishers, Boston. 303 pp.

Sweldens, W. and Schröder, P.: 1996, Building your own wavelets at home, *Wavelets in Computer Graphics*, ACM SIGGRAPH Course Notes, pp. 15–87.

Wackernagel, H.: 1998, *Multivariate geostatistics*, second edn, Springer, Paris.

9. Appendix: 2D average interpolating wavelets algorithm

The average interpolating wavelets algorithm used in our experiments, will presented as a C-implementation The implementation follows the descriptions in Bjørke and Nilsen (2002) and Bjørke and Nilsen (2003), see also applications of the metod in Bjørke and Nilsen (2007; 2009) and Bjørke and Nilsen (2005). The calling syntax of the algorithm is **2dforward(** A, i, j, q **)** where A is a $2^n \times 2^n$ matrix of cell average values, i and j are the number of rows and columns of A, and q the number of levels in the expansion. The following example will clarify the role

of expansion. Assume matrix A_0 as

$$A_0 = \begin{bmatrix} 2.1 & 4.3 & 1.8 & 2.9 \\ 3.5 & 5.8 & 7.1 & 3.2 \\ 8.7 & 3.2 & 7.8. & 3.6 \\ 4.1 & 6.9 & 4.4 & 6.7 \end{bmatrix}$$

with spatial resolution 10m. From this matrix we want to make an expansion to a matrix with spatial resolution 2.5m. This means that we must increase the size of A_0 from 4×4 cells to size 16×16 cells. From A_0 we construct a new matrix A with size 16×16 cells by filling out the extra cells with zeros as

$$A = \begin{bmatrix} 2.1 & 0 & 0 & 0 & 4.3 & 0 & 0 & 0 & 1.8 & 0 & 0 & 0 & 2.9 & 0 & 0 & 0 \\ 0 & 0 & 0 & 0 & 0 & 0 & 0 & 0 & 0 & 0 & 0 & 0 & 0 & 0 & 0 & 0 \\ 0 & 0 & 0 & 0 & 0 & 0 & 0 & 0 & 0 & 0 & 0 & 0 & 0 & 0 & 0 & 0 \\ 0 & 0 & 0 & 0 & 0 & 0 & 0 & 0 & 0 & 0 & 0 & 0 & 0 & 0 & 0 & 0 \\ 3.5 & 0 & 0 & 0 & 5.8 & 0 & 0 & 0 & 7.1 & 0 & 0 & 0 & 3.2 & 0 & 0 & 0 \\ 0 & 0 & 0 & 0 & 0 & 0 & 0 & 0 & 0 & 0 & 0 & 0 & 0 & 0 & 0 & 0 \\ 0 & 0 & 0 & 0 & 0 & 0 & 0 & 0 & 0 & 0 & 0 & 0 & 0 & 0 & 0 & 0 \\ 0 & 0 & 0 & 0 & 0 & 0 & 0 & 0 & 0 & 0 & 0 & 0 & 0 & 0 & 0 & 0 \\ 8.7 & 0 & 0 & 0 & 3.2 & 0 & 0 & 0 & 7.8. & 0 & 0 & 0 & 3.6 & 0 & 0 & 0 \\ 0 & 0 & 0 & 0 & 0 & 0 & 0 & 0 & 0 & 0 & 0 & 0 & 0 & 0 & 0 & 0 \\ 0 & 0 & 0 & 0 & 0 & 0 & 0 & 0 & 0 & 0 & 0 & 0 & 0 & 0 & 0 & 0 \\ 0 & 0 & 0 & 0 & 0 & 0 & 0 & 0 & 0 & 0 & 0 & 0 & 0 & 0 & 0 & 0 \\ 4.1 & 0 & 0 & 0 & 6.9 & 0 & 0 & 0 & 4.4 & 0 & 0 & 0 & 6.7 & 0 & 0 & 0 \\ 0 & 0 & 0 & 0 & 0 & 0 & 0 & 0 & 0 & 0 & 0 & 0 & 0 & 0 & 0 & 0 \\ 0 & 0 & 0 & 0 & 0 & 0 & 0 & 0 & 0 & 0 & 0 & 0 & 0 & 0 & 0 & 0 \\ 0 & 0 & 0 & 0 & 0 & 0 & 0 & 0 & 0 & 0 & 0 & 0 & 0 & 0 & 0 & 0 \end{bmatrix}.$$

By calling **2dforward(**$A, 4, 4, 2$**)**, the function returns a matrix A where the empty cells are filled in with interpolated values.

```
int forward2d(double *matrix,int size_i,int size_j,int numlevels)
{
   int i,j,step,smallstep,level,maxlev,tmp,Tmp,minsize;

   if(size_i<size_j){
      tmp=size_i;
      Tmp=size_j;
   }else{
      Tmp=size_i;
      tmp=size_j;
   }
   minsize=3;
   maxlev=0;
   step=1;
```

```
   while(((tmp%2)==0) && ((Tmp%2)==0) && ((tmp/2)>=minsize) &&
   (maxlev<numlevels)){
      tmp/=2;
      Tmp/=2;
      maxlev++;
   }
   for(level=1;level<=maxlev;level++){
      smallstep=step;
      step*=2;
      for(i=0;i<size_i;i+=smallstep){
         for(j=0;j<size_j;j+=step){
            matrix[size_j*i+j+smallstep]-=matrix[size_j*i+j];
            matrix[size_j*i+j+smallstep]*=0.5;
            matrix[size_j*i+j]+=matrix[size_j*i+j+smallstep];
         }
         matrix[size_j*i+smallstep]-=
            -0.375*matrix[size_j*i]
    +0.500*matrix[size_j*i+step]
    -0.125*matrix[size_j*i+2*step];
         for(j=step;j<size_j-step;j+=step){
            matrix[size_j*i+j+smallstep]-=
               +0.125*matrix[size_j*i+j+step]
      -0.125*matrix[size_j*i+j-step];
         }
         matrix[size_j*(i+1)-smallstep]-=
            +0.125*matrix[size_j*(i+1)-3*step]
    -0.500*matrix[size_j*(i+1)-2*step]
    +0.375*matrix[size_j*(i+1)-step];
      }
      for(j=0;j<size_j;j+=smallstep){
         for(i=0;i<size_i;i+=step){
            matrix[size_j*(i+smallstep)+j]-=matrix[size_j*i+j];
            matrix[size_j*(i+smallstep)+j]*=0.5;
            matrix[size_j*i+j]+=matrix[size_j*(i+smallstep)+j];
         }
         matrix[size_j*smallstep+j]-=
            -0.375*matrix[j]
            +0.500*matrix[size_j*step+j]
            -0.125*matrix[size_j*2*step+j];
         for(i=step;i<size_i-step;i+=step){
            matrix[size_j*(i+smallstep)+j]-=
               +0.125*matrix[size_j*(i+step)+j]
               -0.125*matrix[size_j*(i-step)+j];
         }
         matrix[size_j*(size_i-smallstep)+j]-=
            +0.125*matrix[size_j*(size_i-3*step)+j]
            -0.500*matrix[size_j*(size_i-2*step)+j]
            +0.375*matrix[size_j*(size_i-step)+j];
      }
   }
   return(maxlev);
}
```

Applications and Experiences of Quality Control

Edited by Prof. Ognyan Ivanov

ISBN 978-953-307-236-4
Hard cover, 704 pages
Publisher InTech
Published online 26, April, 2011
Published in print edition April, 2011

The rich palette of topics set out in this book provides a sufficiently broad overview of the developments in the field of quality control. By providing detailed information on various aspects of quality control, this book can serve as a basis for starting interdisciplinary cooperation, which has increasingly become an integral part of scientific and applied research.

How to reference

In order to correctly reference this scholarly work, feel free to copy and paste the following:

Jan Terje Bjørke and Stein Nilsen (2011). Quality Assessments of Seafloor Mapping with Multibeam Echo Sounders, Applications and Experiences of Quality Control, Prof. Ognyan Ivanov (Ed.), ISBN: 978-953-307-236-4, InTech, Available from: http://www.intechopen.com/books/applications-and-experiences-of-quality-control/quality-assessments-of-seafloor-mapping-with-multibeam-echo-sounders

INTECH
open science | open minds

InTech Europe
University Campus STeP Ri
Slavka Krautzeka 83/A
51000 Rijeka, Croatia
Phone: +385 (51) 770 447
Fax: +385 (51) 686 166
www.intechopen.com

InTech China
Unit 405, Office Block, Hotel Equatorial Shanghai
No.65, Yan An Road (West), Shanghai, 200040, China
中国上海市延安西路65号上海国际贵都大饭店办公楼405单元
Phone: +86-21-62489820
Fax: +86-21-62489821